Dynamic neutral beam current and voltage control to improve beam efficacy in tokamaks

D. C. Pace (庞大卫), M. E. Austin, L. Bardoczi, C. S. Collins, B. Crowley, E. Davis, X. Du, J. Ferron, B. A. Grierson, W. W. Heidbrink, C. T. Holcomb, G. R. McKee, C. Pawley, C. C. Petty, M. Podestà, J. Rauch, J. T. Scoville, D. A. Spong, K. E. Thome, M. A. Van Zeeland, J. Varela, and B. Victor

Dynamic neutral beam current and voltage control to improve beam efficacy in tokamaks

D. C. Pace (庞大卫),[1,a),b)] M. E. Austin,[2] L. Bardoczi,[3] C. S. Collins,[1] B. Crowley,[1] E. Davis,[4] X. Du,[5] J. Ferron,[1] B. A. Grierson,[6] W. W. Heidbrink,[5] C. T. Holcomb,[7] G. R. McKee,[8] C. Pawley,[1] C. C. Petty,[1] M. Podestà,[6] J. Rauch,[1] J. T. Scoville,[1] D. A. Spong,[9] K. E. Thome,[3] M. A. Van Zeeland,[1] J. Varela,[9] and B. Victor[7]

[1]*General Atomics, P.O. Box 85608, San Diego, California 92186-5608, USA*
[2]*University of Texas, Austin, Texas 78712, USA*
[3]*Oak Ridge Associated Universities, Oak Ridge, Tennessee 37831, USA*
[4]*Massachusetts Institute of Technology, Cambridge, Massachusetts 02139, USA*
[5]*University of California Irvine, Irvine, California 92697, USA*
[6]*Princeton Plasma Physics Laboratory, P.O. Box 451, Princeton, New Jersey 08543, USA*
[7]*Lawrence Livermore National Laboratory, 7000 East Ave, Livermore, California 94550-9234, USA*
[8]*University of Wisconsin-Madison, Madison, Wisconsin 53706, USA*
[9]*Oak Ridge National Laboratory, P.O. Box 2008, Oak Ridge, Tennessee 37831, USA*

An engineering upgrade to the neutral beam system at the DIII-D tokamak [J. L. Luxon, Nucl. Fusion **42**, 614 (2002)] enables time-dependent programming of the beam voltage and current. Initial application of this capability involves pre-programmed beam voltage and current injected into plasmas that are known to be susceptible to instabilities that are driven by energetic ($E \geq 40\,\text{keV}$) beam ions. These instabilities, here all Alfvén eigenmodes (AEs), increase the transport of the beam ions beyond a classical expectation based on particle drifts and collisions. Injecting neutral beam power, $P_{\text{beam}} \geq 2\,\text{MW}$, at reduced voltage with increased current reduces the drive for Alfvénic instabilities and results in improved ion confinement. In lower-confinement plasmas, this technique is applied to eliminate the presence of AEs across the mid-radius of the plasmas. Simulations of those plasmas indicate that the mode drive is decreased and the radial extent of the remaining modes is reduced compared to a higher beam voltage case. In higher-confinement plasmas, this technique reduces AE activity in the far edge and results in an interesting scenario of beam current drive improving as the beam voltage reduces from $80\,\text{kV}$ to $65\,\text{kV}$. *Published by AIP Publishing.* https://doi.org/10.1063/1.5016160

I. INTRODUCTION

Energetic ions, sourced by beam injection, electromagnetic wave injection, or fusion reactions, serve to heat fusion plasmas and drive current that enables stable confinement. The effects of energetic ions on plasma instabilities and the mechanical issue of power loading to the reactor walls are important issues for future burning plasma devices including the ITER tokamak.[1] Present day tokamak facilities investigate energetic ion transport and various interactions with plasma waves, especially Alfvén eigenmodes (AEs).[2] A detailed overview of the state of energetic ion physics understanding is provided by Heidbrink and Sadler,[3] and a more focused overview of energetic ion interactions with AEs is provided by Breizman and Sharapov[4] [the toroidal Alfvén eigenmode (TAE) and reversed-shear Alfvén eigenmode (RSAE) are the modes of interest in the present work]. The rapid development of this knowledge base is leading to a fresh look on past experiments, e.g., identifying energetic ion transport by instabilities in TFTR plasmas that were not known at the time of the shots.[5]

There is an interplay between the goals of controlling energetic ion transport and improving the efficiency of neutral beam injection. One approach is to affect the instabilities without changing the energetic ion distribution, such as by injecting electromagnetic waves using an antenna as in the JET, C-Mod, and MAST tokamaks,[6] applying global error fields as in NSTX,[7] or by injecting electron cyclotron heating to alter the plasma such that mode damping is changed as in TJ-II,[8] DIII-D,[9] and ASDEX upgrade.[10] Another approach is to change the energetic ion distribution in some manner that reduces the prevalence of instabilities and then propagate some beneficial effect on the particle transport. The injection geometry of neutral beams provides an early decision point that will necessarily instill some limitation in what can be achieved with the beams. The addition of new beamlines with the increased radial tangency radius was found to stabilize some instabilities in NSTX-U,[11] while the nearly perpendicular (to the magnetic field) orientation of the W7-X neutral beam prevents it from being used for plasma startup.[12] Modifying existing neutral beams to enable time-variable current and voltage control provided for improved beam ion velocity space manipulation on DIII-D.[13]

The present work considers another way of tailoring the beam ion distribution: changing the current and voltage of

---

the neutral beams simultaneously. For beam ions existing at velocities below the Alfvén speed of the plasma, the ion-AE energy exchange occurs at higher order resonances with a strong dependence on the ion velocity.[14] Given any particular plasma conditions, it should be possible to identify a beam voltage that minimizes the AE drive. From an engineering perspective, the power output of the beams is directly related to the voltage; therefore, any changes in voltage would also change the beam power. Independent control of neutral beam voltage and current enables a new operating mode in which power can be maintained across a range of voltages, i.e., the same power can be produced at different values of beam ion velocity. This opens up a wide range of experimental possibilities, with two examples shown here.

The results are organized as follows: Sec. II describes the DIII-D neutral beam system and engineering changes that enabled time-variable current and voltage, Sec. III describes the reduction of high frequency plasma instabilities in low-confinement (L-mode) plasmas, Sec. IV includes results of increased neutral beam current drive in high-confinement (H-mode) plasmas, and then Sec. V summarizes the conclusions.

II. NEUTRAL BEAMS AT DIII-D

A. System parameters

The DIII-D neutral beam system provides upwards of 20 MW of power for heating and driving current in the plasma. The beams inject ions across a range of energies (beam voltage), E_{beam} approximately described by, $40 \leq E_{\mathrm{beam}} \leq 85$ kV with currents ranging across $40 \leq I_{\mathrm{beam}} \leq 65$ A. Injected neutral species can be hydrogen, deuterium, or helium. Each of the eight separate beams can modulate with minimum 5 ms on/off periods. The plasma control system (PCS) uses this modulation capability to enable real-time feedback of plasma stored energy and/or injected beam torque.

Figure 1 is a scaled drawing that provides the injection geometry of the eight separate beamlines (projected onto the midplane) and demonstrates their physical scale. These beams also serve many diagnostic purposes as there is no single lower-power diagnostic beam. The 150° beamline
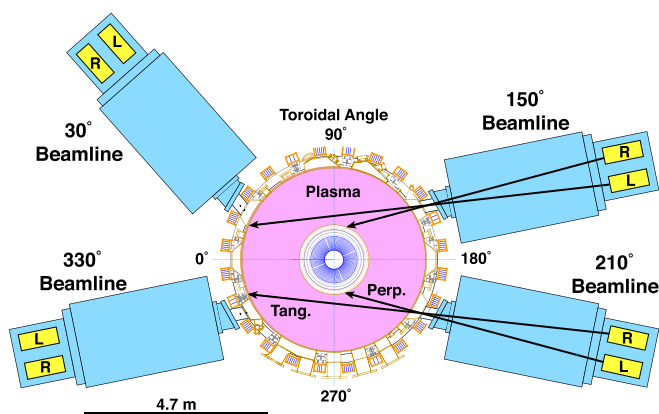

FIG. 1. Schematic of the DIII-D neutral beam system. Example beam injection geometries are labeled for tangential (Tang.) and perpendicular (Perp.) beamlines. Individual beams are named according to their toroidal position and their orientation within the main housing, e.g., 30L.

(containing the 150 L and 150 R neutral beams as indicated in Fig. 1) is capable of tilting vertically[15] to allow off-axis injection (it remains fixed at a single angle throughout the shot). Off-axis neutral beam injection has been well characterized,[16] and modeling of neutral beam current drive was most recently established through an international effort encompassing many different facilities.[17]

Additional flexibility is provided by the 210° beamline, which is directed in the opposite toroidal direction compared to the others.[18] This orientation allows for the injection of counter-current (counter to the plasma current) beam injection regardless of the present direction of the plasma current. While beam injection in the counter-current direction is subject to increased prompt loss levels compared to co-current injection, it remains a powerful actuator for driving rotation and heating plasmas[19] and it was a fundamental component of the discovery of the improved confinement regime known as QH-mode.[20]

B. In-shot control of beam current and voltage

A fundamental improvement in tokamak capability is achieved by keeping the injected power of a single neutral beam source fixed while its current and voltage change with time. This allows the total power to the plasma to remain constant as the physics actuators of beam ion energy (voltage) and number density (current) change. Adding the capability for the neutral beams to change their current and voltage during plasma shots was not an obvious engineering upgrade because limitations in beam divergence require the injected beam power change along with the current and voltage. This requirement is described by a parameter known as the perveance, Π, which is related to the beam current, I, and voltage, V, as $\Pi = I/V^{3/2}$. The technical changes required to achieve variable perveance are discussed in other publications,[21,22] while the physics implications are provided here.

The neutral beams function by extracting ions from a filament-based plasma source, accelerating the ions through the desired voltage, passing them through a large gas chamber to neutralize a fraction of them (dependent on the accelerating voltage), and then collimating the resulting neutral stream as it enters the tokamak. The perveance indicates the extent to which space charge affects the extraction of the particle beam. Electrostatic fields arising from space charge deflect the accelerated particles away from the ideal path that expels those particles in a desired, focused, direction. In practice, there is a value of perveance for any given DIII-D neutral beam that represents the minimum space charge influence on the path of the accelerated ions. At this perveance, therefore, the ions experience the least deflection away from the desired path into the tokamak and the beams inject at the minimum divergence. The final gridded apertures of the neutral beams are 12 cm wide by 48 cm tall, so it is the vertical divergence that is of greater concern for ensuring that injected neutrals reach the plasma instead of scraping off along the walls of the beam duct or vacuum vessel port. Only vertical divergence is presented here. Typical perveance operating values are in the vicinity of $2.3 \times 10^{-6} \leq \Pi \leq 3.0 \times 10^{-6}$ (AV$^{-3/2}$). Independent control of neutral

beam current and voltage necessarily allows the system to operate away from its optimum perveance and hence the phrase used to describe this operating method: Variable Beam Perveance (VBP).

If the focus of a neutral beam needs to be held fixed, i.e., a minimum divergence maintained, then any changes to either the beam current or the voltage will be limited by their ratio, Π. The consequence is that any intention to vary the beam current or voltage with time would also change the injected power. Two available operating modes are

- Voltage Change with Auto-perveance: the voltage is pre-programmed and the on/off modulation can be programmed separately, i.e., the voltage will follow its program regardless of whether the beam is being modulated. The Plasma Control System (PCS)[23] automatically adjusts the beam current to enforce a specific value of optimum perveance.
- Voltage and Current Change: both the beam voltage and current are pre-programmed. If the resulting perveance is too far away from optimum, then the beam will stop injecting. This stop-point is determined by a machine protection circuit that measures stray ion impacts into other parts of the neutral beam system. Experience shows that this allowable perveance range is approximately 15% from optimum.

Both operating modes provide a maximum voltage slew rate of 40 kV/s and a range of variation within a single shot of $\Delta V = 20$ kV. The single-shot range limit is born of the way in which the power supplies set the acceleration voltage and this cannot be changed without a major hardware replacement.

C. Perveance effect on beam divergence

Considerations for implementing VBP must include an assessment of how increased beam divergence will affect device operation. Beam modeling, including divergence,[24] can be used to demonstrate that protection circuitry prevents the beams from firing in a state featuring dangerous divergence values. Aside from machine protection, it is desirable to maintain a low divergence in order to maximize the beam driven current and resultant plasma heating. In experiments, the beam divergence can be measured within the beam itself through a Doppler spectroscopy technique that makes use of an existing Multichord Divertor Spectroscopy diagnostic system.[25]

Measured divergence as a function of beam voltage is shown in Fig. 2. This shot featured the VBP mode of changing both the current and voltage in order to maintain constant power. The divergence, Θ, is observed to vary across a range $1.4° \leq \Theta \leq 2.0°$, where $\Theta = 1.4°$ is consistent with the previously determined minimum value. Divergences above $2°$ will generally lead to a trip of the neutral beam protection circuit and are therefore not expected to be produced in experimental conditions. More detailed consideration of the effect of beam divergence in power balance calculations is provided in the Appendix.
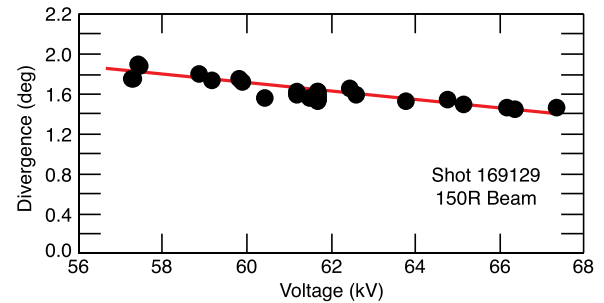

FIG. 2. Measured vertical divergence of the 150R neutral beam as a function of beam voltage in a scenario wherein the beam perveance is not held constant.

III. REDUCED ALFVÉN EIGENMODE ACTIVITY IN L-MODE PLASMAS

There is a physics motivation to test VBP in easily reproducible plasmas that are conducive to modeling and simulation. Such an experiment is designed around a base of an oval-shaped plasma that is physically limited against the center post with plasma parameters of toroidal magnetic field $B_0 = 2.0$ T, plasma current $I_p = 0.5$ MA, and vertical elongation $\kappa = 1.6$. This regime, utilizing injected neutral beam power levels between 1 and 10 MW and some variation in elongation, is the basis for many DIII-D investigations into Alfvén eigenmode stability and resulting beam ion transport. These include beam ion losses due to core-localized reversed-shear AEs,[26] AE stability for predictions of ITER behavior,[27] AE drive from beam ions that complete only a single poloidal circuit,[28,29] and the critical gradient nature of beam ion transport.[30]

It is emphasized that this experiment focuses on understanding the physics behind the wave-ion interactions that allow injected beam ions to drive Alfvénic instabilities. As such, this experiment included a secondary effort to perform engineering checks on the VBP implementation. Some of the instability results may have been similarly produced with constant voltage injection; however, varying the injected beam parameters in these L-modes helped to prepare the system for the H-mode experiments discussed later.

The experiment consists of reproducing an L-mode plasma with approximately 2.5 MW of injected beam power with minimal beam modulation and the largest possible variation in beam voltage. Radial profiles of the resulting plasma parameters are shown in Fig. 3. These profiles are representative across multiple shots and are used in all AE simulations. From the profiles, it is possible to classify this plasma as low density [Fig. 3(a)] with a significant beam ion pressure contribution [Fig. 3(b)], and a reversed-shear high q-profile [Fig. 3(c)] that is conducive to producing AEs.

The full neutral beam heating for these plasmas involves two neutral beams injecting continuously during the first second of the shot (taking advantage of the high-q period when plasma current is still moving inward from the edge). These beams (150L and 150R, see Fig. 1) are directed on-axis and execute a voltage change from 56 kV to 69 kV over approximately 500 ms. Two other neutral beams inject widely spaced pulses of 10 ms duration for diagnostic purposes.
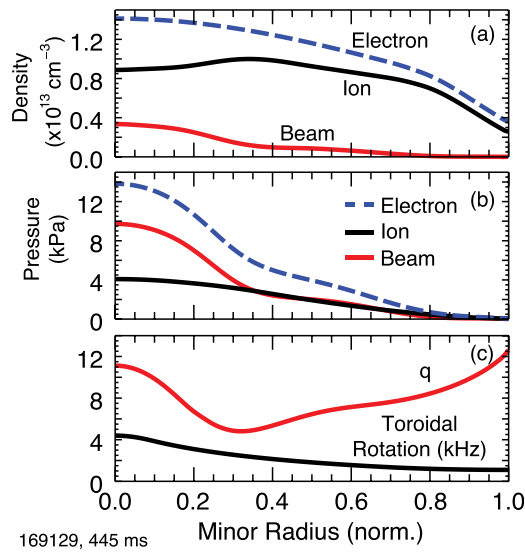
FIG. 3. Plasma parameters from the L-mode experiment as used by the FAR3D code. (a) Electron, ion, and beam density. (b) Electron, ion, and beam pressure. (c) Toroidal rotation and q-profile.

Figure 4 shows the beam voltages and the total injected beam power for a shot that begins with lower voltage (169128, red trace) and a comparison shot beginning with higher voltage injection (169129, black trace). Total beam power is well matched across this time period. A brief, but large, increase in total beam power is present over $640 \leq t \leq 660$ ms when two neutral beams inject at 80 kV for diagnostic purposes.

Differences in the AE spectra produced by these plasmas are indicated by the spectrograms in Fig. 5. These spectrograms represent a global overview of the density fluctuations in the plasma because the cross-power is calculated between
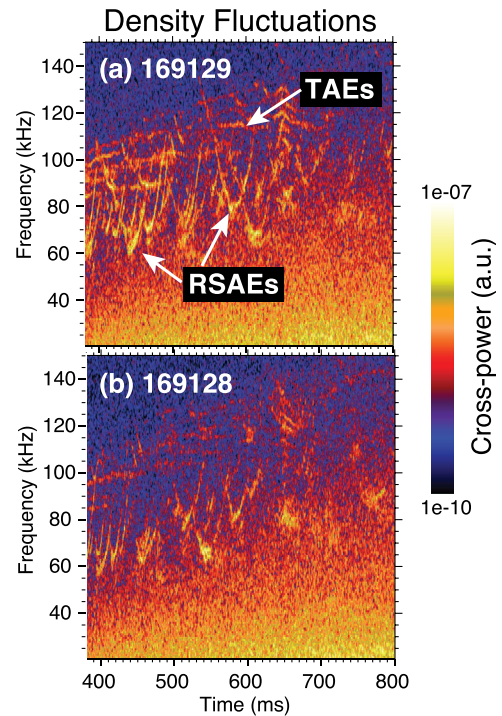
FIG. 5. Cross-power of density fluctuations from two interferometer chords for (a) shot 169129 and (b) shot 169128.

vertical and horizontal interferometer chords,[31] which are measurements of line-integrated density and its fluctuation. Both shots show fluctuations in the frequency range of 50–150 kHz, with the upward frequency sweeping RSAEs and the nearly fixed frequency TAEs indicated by annotations. The same amplitude color scale is used in each panel, indicating that the initially higher voltage shot of Fig. 5(a) features larger TAE amplitude and longer-lived RSAEs compared to the initially lower voltage shot of Fig. 5(b).

After 700 ms, the AE activity nearly disappears from both shots, which is caused by the continued decrease in the q-profile as the plasma current penetrates. This is only coincidental with the cross-over of the beam voltages as shown in Fig. 4. In similar shots with greater neutral beam power, it is possible to continue to drive AEs beyond the 1000 ms mark.[32] As shown in Sec. IV, AEs are regularly produced in shots featuring moderate neutral beam heating and q-profiles with minimum values (q_{min}) just above 2.

While the apparent number density and amplitude of AEs are reduced in the lower voltage shot, the observed spatial extent of the modes is also different between the two plasmas. Figure 6 is a cross-power of electron temperature fluctuations incorporating multiple points from the electron cyclotron emission diagnostic system.[33] All of these measurements are acquired within a range of normalized minor radius, ρ, given by $0.4 \leq \rho \leq 0.7$ and therefore represent the presence of instabilities in the mid-radius of the plasma. The higher beam voltage case shown in Fig. 6(a) features well defined fluctuations associated with TAEs. By comparison, the lower voltage shot of Fig. 6(b) provides only hints of equivalent fluctuations.

Purposely affecting the spatial extent of instabilities can be a useful tool for controlling transport levels in a tokamak
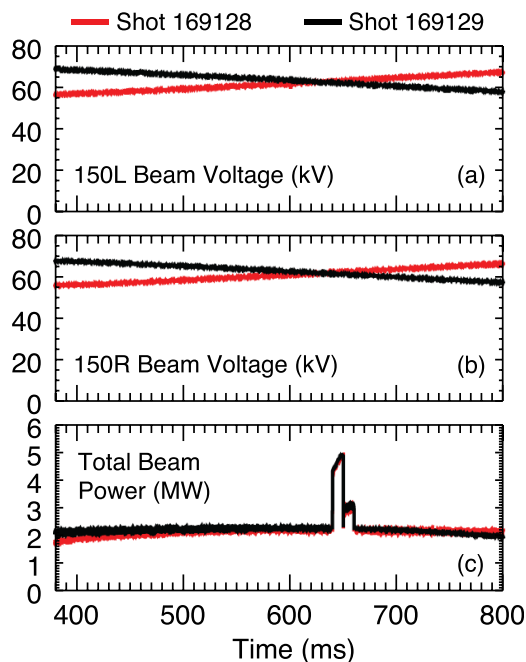

FIG. 4. Neutral beam behavior for the L-mode experiment comparing shots 169128 (red) and 169129 (black). (a) Voltage of 150L neutral beam. (b) Voltage of 150R neutral beam. (c) Total injected neutral beam power.
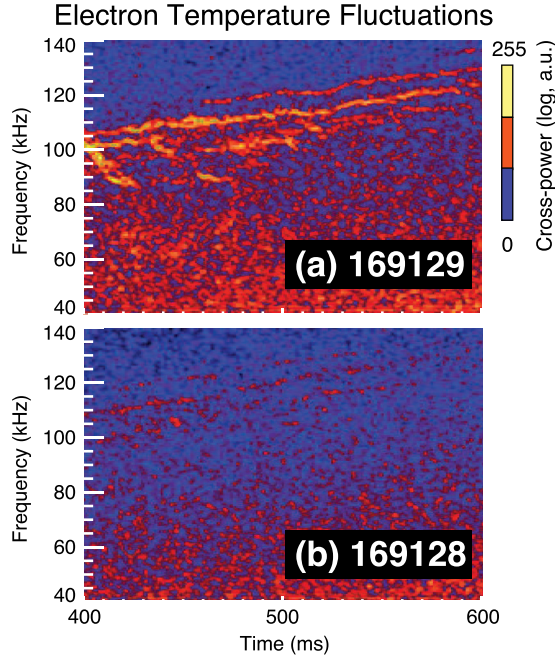
FIG. 6. Cross-power between electron temperature measurements within the radial region of $0.4 \leq \rho \leq 0.7$ for shots (a) 169129 and (b) 169128.

FIG. 7. Frequency and growth rates of identified (a) $n = 3$ and (b) $n = 4$ modes calculated by FAR3D using the plasma profiles of Fig. 3. Modes are identified in the frequency range of 50–150 kHz. Unstable modes are identified with red circles, and stable modes are represented by black circles.

plasma. Experiments[34] and simulations[35] indicate that the resulting energetic ion transport due to Alfvénic instabilities is largely determined according to the amount of spatial overlap of the AEs. Even if the amplitude of the AE spectrum was largely unaffected by reduced beam voltage, an improvement in beam ion confinement may still result from the reduced overlap of the remaining modes.

This plasma scenario is simulated with the FAR3D[36] code to examine the theoretical changes in AE stability and eigenstructure as a function of the variable beam perveance. FAR3D solves the reduced, non-linear, resistive MHD equations including linear wave-ion resonances. It identifies the most unstable mode, i.e., the mode with the largest growth rate, and includes the beam ion population as a high temperature Maxwellian distribution. The input plasma profiles for these simulations are shown in Fig. 3.

Figure 7 shows the calculated growth rate for the $n = 3$ and $n = 4$ modes as a function of beam ion energy. Here, the beam ion energy is recorded as the velocity of the beam ions compared to the Alfvén velocity, $\langle v_{fast} \rangle / v_{Alfven}$, where $\langle v_{fast} \rangle$ is the effective temperature of the beams ions and v_{Alfven} is set by the plasma parameters and remains constant across simulations. The eigensolver of FAR3D searches for modes in the frequency range of $50 \leq f \leq 150$ kHz. Of these identified modes, the range of frequency does not change significantly across the scan of beam ion energy. Modes with negative growth rates are stable and indicated by black circles in the figure. Unstable modes feature positive growth rates and are represented by red circles. While a trend in the growth rates is not apparent, there appears to be a threshold effect resulting in the complete lack of unstable modes for $\langle v_{fast} \rangle / v_{Alfven} < 0.06$. The growth rate decrease is the result of reduced resonant drive (again, plasma terms such as the mode damping are constant across simulations).
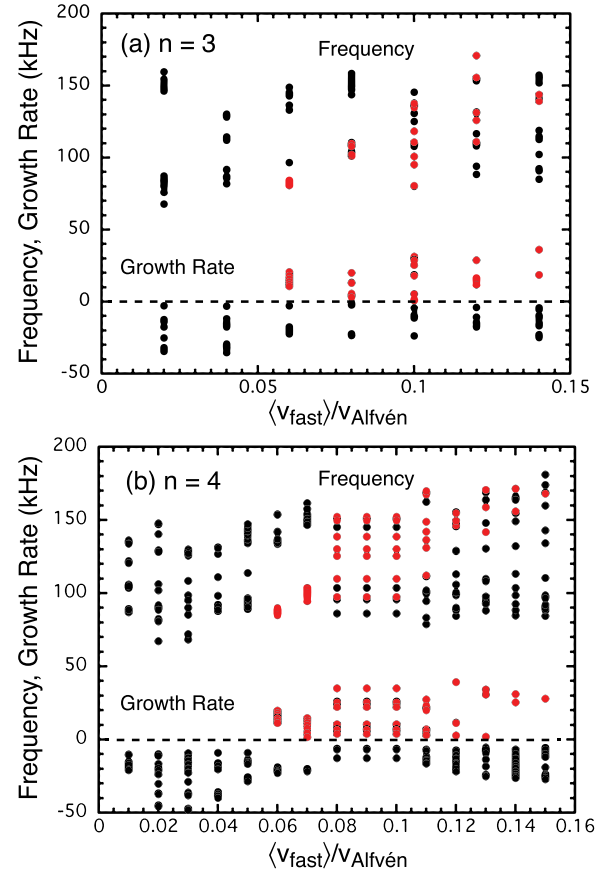
Beam ion velocity effects on the spatial structure of the modes are shown in Fig. 8. These two panels display the calculated eigenstructure (potential fluctuation amplitude) for the $n = 3$ case over approximately a factor of two in beam ion velocity. Figure 8(a) shows a radially extended mode structure at $\langle v_{fast} \rangle / v_{Alfven} = 0.14$, and Fig. 8(b) shows a considerably narrower mode structure at $\langle v_{fast} \rangle / v_{Alfven} = 0.06$. This result is consistent with the observed reduction (nearly complete reduction) of AE activity in the mid-radius region as presented in Fig. 6.

As these L-mode plasmas were produced at 2 MW of input beam power, the level of beam ion transport remained close to classical. The purpose of the experiment is to test the hypothesis that controlled beam current and voltage can be used to produce a fixed amount of injected power while reducing the prevalence of Alfvénic instabilities. Having confirmed that hypothesis, an application of this capability is demonstrated in the H-mode scenario of Sec. IV.

IV. INCREASED BEAM CURRENT DRIVE IN HIGH q_{min} SCENARIO

The steady state tokamak scenario known as "high q_{min}" features $q_{min} > 2.0$ and has been extensively investigated at DIII-D[37] and EAST.[38] The experiment begins with the same plasma characteristics of Holcomb *et al.*,[37] $B_0 = 1.7$ T, $I_p = 0.8$ MA, $\kappa = 1.8$, and line-integrated electron densities,
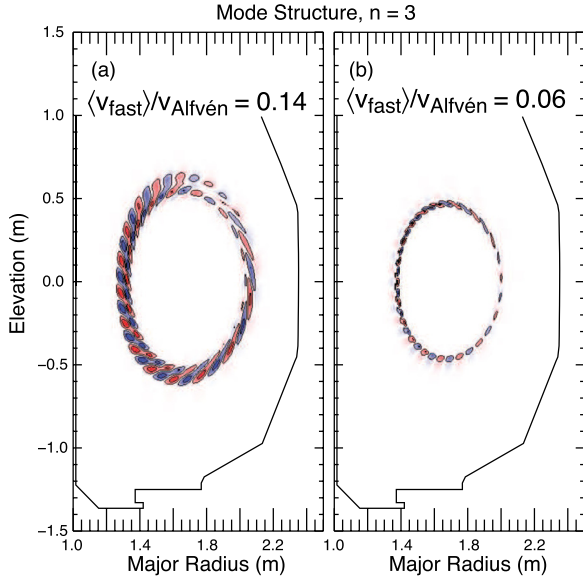
FIG. 8. FAR3D calculation of the spatial structure (potential fluctuation amplitude) of the most unstable mode at $n=3$ for normalized beam ion velocities of (a) $\langle v_{fast}\rangle/v_{Alfven} = 0.14$ and (b) $\langle v_{fast}\rangle/v_{Alfven} = 0.05$.

FIG. 9. Time evolution of the (a) normalized β, (b) neutral beam power, and (c) voltage of the 150L neutral beam for two high q_{min} shots with different beam voltage programs.

n_e, in the range of $2.4 \leq n_e \leq 3.4 \times 10^{19}$ m^{-3}, and then implements variable beam perveance to compare beam efficacy at similar powers but different voltages. The total injected beam power is approximately 7 MW. The 150° neutral beam is injected at its maximum off-axis tilt angle and Alfvén eigenmode stability in the presence of off-axis beams is well known.[39]

In contrast to the plasmas discussed in Sec. III, the shots presented here feature the same neutral beam injection characteristics through $t = 2500$ ms. Three neutral beams were available for VBP in these shots (there are seven beams capable of VBP presently), with two of those beams injecting off-axis. The plasma stored energy is controlled in the feedback mode by the PCS and the variable perveance beams operate at 70 kV. Over $2500 \leq t \leq 3000$ ms (annotated in later figures as the Beam IV Change period), the so-called lower voltage shots execute VBP programs that decrease voltage to 65 kV or lower while increasing the beam current to reach 7 MW of total injected power. The higher voltage shots execute a pre-programmed waveform that takes the beams to 80 kV while decreasing the beam current.

Temporal waveforms for two shots are shown in Fig. 9. The line-integrated electron density averaged $\bar{n}_e = 3.4 \times 10^{19}$ m^{-3} in the higher voltage shot, compared to the value of $\bar{n}_e = 2.4 \times 10^{19}$ m^{-3} in the comparison shot. Differences in plasma behavior related to this density inequality are accounted for by the TRANSP[40] analysis and modeling code. Note that the greater density of the 80 kV shot should improve beam ion confinement by facilitating slowing down of the injected particles. The slowing down time in the core of the 80 kV shot is approximately 90 ms, which is 18% shorter than the 110 ms slowing down time of the 65 kV shot. Figure 9(a) shows that both shots feature normalized β values at 2 or greater. The total injected neutral beam power is shown in Fig. 9(b), and it differs by 0.3 MW (4%) in these shots. Figure 9(c) shows the voltage evolution of the 150 L neutral beam.
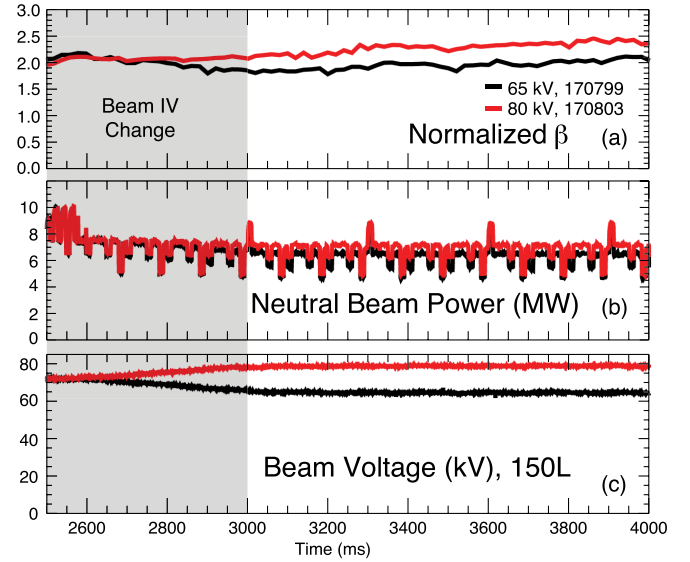
Modeling of the beam ion transport is accomplished using the TRANSP code. TRANSP features an operating mode in which it varies an *ad hoc* beam ion diffusivity, D_B, as needed to match the measured neutron rate from the plasma. This provides a good indication of the level of beam ion transport because the largest contributor to deuterium-deuterium (DD) fusion is beam-plasma fusion (peak electron temperatures are below 4 keV). This concept is generally applied to beam heated tokamak plasmas and was most recently detailed in a study from MAST.[41] A TRANSP calculation in which $D_B = 0$ represents the classically expected level of beam ion transport, i.e., transport resulting from collisions, charge exchange, and particle drifts. The classical calculations are denoted "No Modes" as they represent the expected behavior if there were no plasma instabilities affecting the beam ions. The use of the OMFIT[42] codebase in executing these calculations greatly improves the flexibility and organization as multiple shots and different modeling setups are implemented.

Figure 10 provides an example of the D_B effect on the neutron rate. Figure 10(a) compares the measured neutron rate (black trace) with the classical expectation ($D_B = 0$, *No Modes*, dashed blue trace) and the result of the TRANSP-identified optimum D_B value (*With Modes*, red trace). The classically expected neutron rate is 50% higher than the measured rate. TRANSP is fully capable, however, of identifying the value of D_B necessary to match the measured rate. This time-varying value of D_B is provided in Fig. 10(b) with the appropriate *With Modes* label.

A comparison of the D_B values deduced from the neutron rates is given in Fig. 11 for the lower and higher beam voltage shots. For $t < 2500$ ms, the values are equal, and then they both plummet during the initial beam voltage change. It is a common, and unexplained, observation that measures of plasma performance transiently improve during the beginning of a VBP period. It remains to be determined whether this is an authentic result of the changing plasma heating,
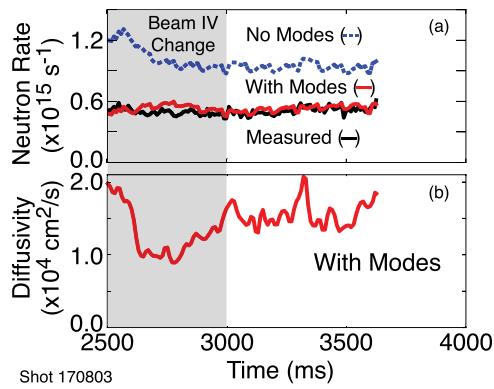
FIG. 10. (a) Neutron rate as measured in shot 170803 (black trace) and as calculated by TRANSP assuming classical beam ion transport ($D_B = 0$, dashed blue trace) and when time-evolving D_B to match the measured rate (red trace). (b) The resulting diffusivity necessary to achieve the best match to the experimental neutron rate.

e.g., possibly due to increased rotational shear as the radial profile of beam torque changes, or some more mundane issue related to modeling of the initial evolution. Regardless, the D_B values reach different stable values across the stationary period of $t > 3000$ ms. Within that time period, the beam ion diffusivity of the higher beam voltage shot is approximately twice that of the lower beam voltage shot.

An example of the sensitivity of the neutron rate to the beam ion confinement is also provided in Fig. 11. The brief spikes occurring at $t = 3000$ and 3300 ms result from 10 ms wide pulses of the 30 L neutral beam at 81 kV. The temporary increase in beam power at high voltage serves to drive fluctuations that cause transport of the greater beam ion population. Of interest to note is that the change in D_B from this high energy beam pulse reduces with time for the lower beam voltage shot. While the $t = 3000$ ms pulse of 30 L increases beam ion diffusivity from $D_B = 0.80 \times 10^4$ cm^2/s to 1.5×10^4 cm^2/s (53% increase), the second pulse at $t = 3300$ ms only increases it from $D_B = 0.75 \times 10^4$ cm^2/s to $D_B = 1.00 \times 10^4$ cm^2/s (25% increase). This is qualitatively consistent with the idea that the lower beam voltage shot has

a smaller population of high energy beam ions because they are sourced only by the 30 L pulse. By comparison, shot 170803 features multiple beams near 80 kV injection and that provides a much larger population to be affected by the additional instability drive of the 30 L pulse. The 3000 ms pulse of 30 L in shot 170799 produces nearly the same change in D_B as shot 170803 because the slowing down of the 70 kV beam ions has not been completed, i.e., both shots feature a more similar beam ion distribution at 3000 ms.

The fluctuation spectra between these higher and lower beam voltage shots demonstrate one obvious difference: an 80 kHz mode appears only in the higher beam voltage plasma. Figure 12 is a spectrogram of density fluctuations measured with the beam emission spectroscopy diagnostic system (BES).[43] This cross-spectrum includes BES positions at normalized minor radii, ρ, of $\rho = 0.7$ and $\rho = 0.9$. Figure 12(a) annotates the spectrogram to indicate the TAE frequency range of $150 \leq f \leq 220$ kHz and the 80 kHz mode that is unique to the higher beam voltage shot. The immediate, and brief, reduction in fluctuations across $f \leq 100$ kHz following the appearance of an edge localized mode (ELM) is indicated in Fig. 12(b). In addition to the presence of the 80 kHz mode, the higher beam voltage shot features larger amplitude TAEs that reappear along with the recovery of the 80 kHz mode after each ELM.

Spatial profiles of the fluctuations are shown in Fig. 13. The TAEs are once again indicated in Fig. 13(a), where the 80 kHz mode is labeled as the *Edge Mode*. These spectrograms are produced using BES across a spatial array over $0.3 \leq \rho \leq 1.0$ at $t = 3500$ ms in both shots. A striking difference is that the higher beam voltage shot of Fig. 13(a) shows much greater fluctuation power in the frequency range $f \leq 100$ kHz compared to the lower beam voltage shot. There are indications of coupling between the 80 kHz mode and the TAEs near 200 kHz in Fig. 13(a), and the radial extent of that triplet of modes is suitable for increasing the transport of beam ions. Reduced fluctuation amplitudes and radial extent in the lower beam voltage shot of Fig. 13(b) are important for achieving improved beam ion confinement in this scenario featuring off-axis beam injection and a large population of beam ions seeded within the mid-radius region.
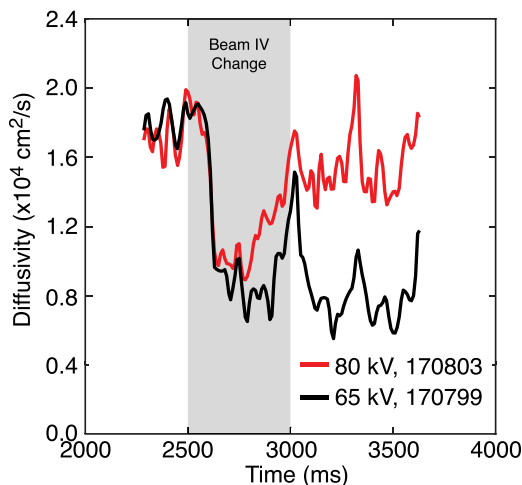

FIG. 11. Beam ion diffusivity calculated by TRANSP as necessary to produce the measured neutron rates in the higher voltage (red trace) and lower voltage (black trace) high q_{min} shots.
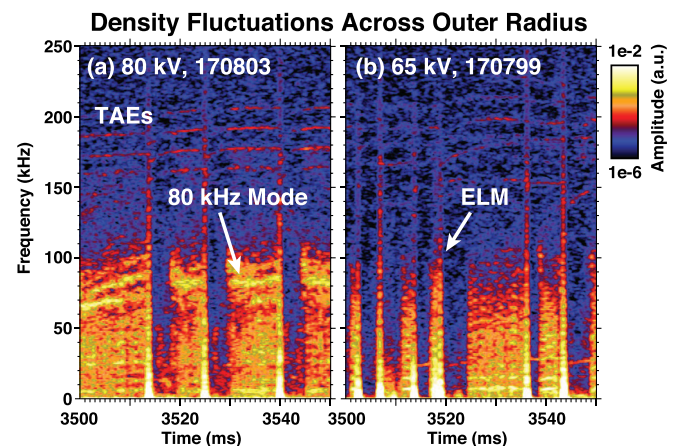

FIG. 12. Cross-power spectrograms of density fluctuations at $\rho = 0.7$ and $\rho = 0.9$ for (a) shot 170803 and (b) shot 170799.
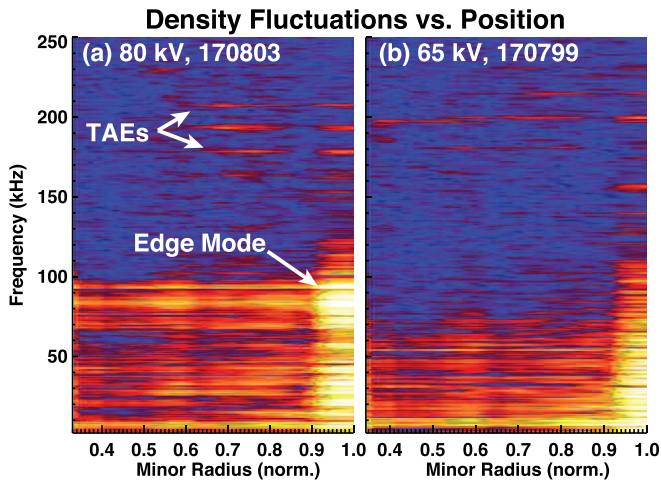
FIG. 13. Spectrograms of density fluctuations for (a) shot 170803 at $t = 3550$ ms and (b) shot 170799 at $t = 3530$ ms.

The realized improvement in neutral beam application comes in the form of increased beam current drive for the lower beam voltage plasma. Figure 14 displays the calculated beam current drive density for the two high q_{min} shots of this section and an additional shot that injected beams at 50 kV or lower through the stationary period. While the 50 kV shot utilized the same stored energy feedback as the other shots of interest, the voltage range limitation of the beams required that it begin injection ($t \leq 2500$ ms) at 55 kV and it is not an exact reproduction of the conditions of the other shots. For the sake of this current drive example, however, it demonstrates an interesting feature of reduced voltage beams.

The neutral beam driven current density plots are separated into two results. Figure 14(a) shows the current drive density for these three cases using the TRANSP modeling of classical beam ion transport, $D_B = 0$. This display therefore accounts for any expected differences in the beam current
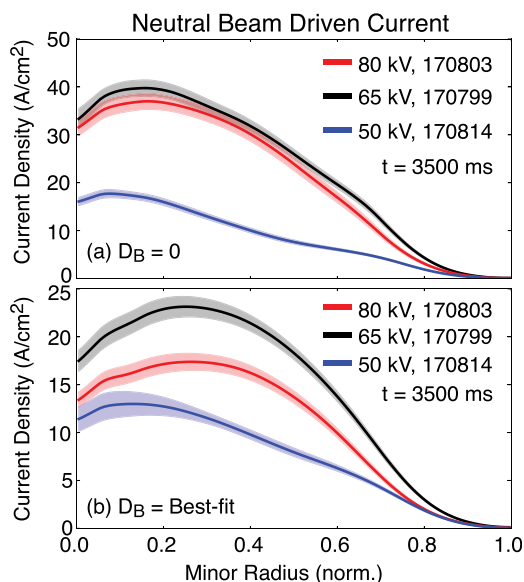

FIG. 14. Calculated total neutral beam driven current three shots with different voltage beam injection for the (a) classical-transport case of $D_B = 0$ and (b) $D_B = $ Best-fit to match measured neutron rate.

drive due to small differences in plasma parameters, e.g., beam current drive should be increased at lower plasma density as experienced in the lower beam voltage shot. Under the classical expectation, the beam current drive of the higher and lower beam voltage shots should be equivalent. Classically, the slightly better beam current drive in the 65 kV shot arises from the 30% lower plasma density compared to the higher voltage shot. At the same densities, the current drive would reduce as the beam voltage reduced. Setting the beam voltage to 50 kV results in a large reduction of the current drive entirely due to the reduced velocity and increased edge deposition of those beams.

Accounting for the beam transport effect of plasma instabilities leads to a very different outcome. Figure 14(b) shows that the lower beam voltage case at 65 kV actually produces a better beam current drive scenario than the 80 kV case. The entire panel of Fig. 14(b) is one-half scale compared to Fig. 14(a), so this result is not an indication of the complete eradication of instability-related beam efficacy reductions. Seeing as how the lowest beam voltage case at 50 kV has closed some of the gap to compete with the 80 kV case, however, does confirm that the transport effect of instabilities is sensitive to the velocity and orbit topology of beam ions. This result is also consistent with experiments and modeling that showed that instabilities can account for large reductions of neutral beam current drive in NSTX.[44] This phenomenon is well suited to further investigation by simulations that incorporate a full beam ion velocity space distribution. Neutral beam current drive is strongly dependent on the orbit topology of the beam ions and is best examined by considering transport within velocity space. One promising method for approaching this topic is to use the Kick Model[45] integrated into TRANSP to apply AE-induced beam ion transport to more finely resolved areas of velocity space. This has been done for some DIII-D experiments and provided more detailed computations of the resulting beam current drive.[32]

It is also clarifying to consider this result in the context of beam ion transport due to micro-instabilities, i.e., broadband turbulence. While initial theoretical and experimental work claimed to show that beam ion current drive was noticeably reduced by the presence of microturbulence, later work from ASDEX Upgrade[46] and DIII-D[47] demonstrated that this was not an actual effect. The concept of microturbulence-induced energetic ion transport is well demonstrated to have an inverse energy dependence in basic plasma devices.[48,49] Such a dependence suggests that reduced neutral beam voltage is even more likely to suffer enhanced diffusion compared to higher beam voltage plasmas. In that regard, then, the present results further demonstrate the lack of microturbulence-induced energetic ion transport in the parameter space of present tokamaks.

V. CONCLUSIONS AND DISCUSSION

Dynamic neutral beam voltage and current control can allow the injected beam ion population to evolve along with plasma characteristics in order to minimize the drive of Alfvén eigenmodes and other instabilities that enhance beam ion transport beyond the classically expected (i.e., considering particle

drifts and collisions) level. The trivial achievement of this capability might see the injected beam power change along with the voltage, but independent beam voltage and current control allows a wider range of beam voltages to produce the same amount of total power. Producing the same power at different values of beam current and voltage increases the beam divergence above the minimal value originally designed into the system. This increase reaches up to approximately $0.5°$ in the DIII-D case, which is acceptable in terms of machine protection and allows 20 kV beam changes in a shot with a slewing rate of 40 kV/s across a range of beam current changes. The process of changing beam current and voltage outside of the optimum ratio (perveance, given by $\Pi = I/V^{3/2}$) is called Variable Beam Perveance (VBP).

Variable beam perveance has been applied to L-mode plasmas in DIII-D by comparing the same 2 MW of injected beam power at different values of beam voltage and current. Importantly, this is accomplished without using power modulation techniques, and a stationary plasma condition is obtained. With beam injection at 80 kV, radially extended toroidal Alfvén eigenmodes (TAEs) are produced, but this group of modes is not present in a similar shot taken with 65 kV beam injection. Simulations that include ion-AE resonant interactions show that the AE drive reduces as the beam voltage is reduced and that the modes excited at 65 kV are localized closer to the plasma core.

The VBP technique is then applied to a high q_{min} steady state scenario plasma. At 7 MW of injected beam power and off-axis injection from two of the beams, a comparison is made between 80 kV and 65 kV injection. The 80 kV case produces considerable mode activity in the far edge of the plasma and this includes greater edge TAE activity compared to the 65 kV case. Modeling shows that the neutral beam driven current is greater at 65 kV injection than at 80 kV, in contrast to classical expectations.

A conceptual summary of these results is that using reduced beam injection voltage to reduce plasma instabilities is only viable if implemented as VBP; otherwise, the reduced beam voltages always require a similar reduction in the total power injected. By increasing the beam current during a voltage reduction, it is possible to maintain the same power level produced in a higher voltage shot, i.e., VBP allows for the injection of a greater number of lower energy neutrals. Next steps for this concept should involve determinations of the ion-AE resonance space in ITER configurations to determine whether a VBP-like technique might be useful for affecting the instability spectrum excited by ITER's 1 MeV neutral beam injection or actively damping AEs generated by 3.5 MeV fusion born alphas. For present machines, modeling and simulation can be used to identify new applications of VBP by identifying regimes in which increased slew rates or greater voltage and current excursions can respond to plasma evolution in real-time.

ACKNOWLEDGMENTS

APPENDIX: BEAM DIVERGENCE IN TRANSP

The creation of time-dependent neutral beam current and voltage was masterfully handled by the TRANSP team. While the temporal evolution of beam voltage and power was already possible in TRANSP, the beam divergence remains a scalar value that is set in the namelist (TRANSP setup file). This means that the beam divergence is modeled at its minimum value throughout the calculation. While Fig. 2 demonstrates that the change in vertical divergence is small, the resulting changes in beam deposition and orbit topology are not themselves obviously small, i.e., the beam ion velocity space distribution may change in meaningful ways. To investigate this technical issue, a series of TRANSP calculations were run at different values of beam divergence for all beams that enacted VBP behavior on a shot of interest.

Figure 15 shows results of neutral beam ion density and driven current density at two different values of vertical beam divergence. The divergence of the individual beams varies little, so the reported standard value is 1.3°. The standard value is compared to an artificial doubling that produces a divergence of 2.5°. The measured excursion of divergence never reaches a value as high as 2.5°, so this modeling is intended to provide a worst-case scenario for any inaccuracies resulting from the static divergence in TRANSP. In Fig. 15(a), it can be seen that the radial profile of beam ion density is within the uncertainty ribbon for these two divergence values. Figure 15(b) shows the same result for the radial profile of beam driven current density. The trend is certainly that the beam driven current is reduced as the divergence increases, which is expected since a more poorly focused beam must be sending more neutrals into the surrounding physical structures and seeding ions in the far edge of the plasma where current drive efficiency is minimal.

Figure 15(b) shows the temporal evolution of the beam driven current density beginning with the initial VBP period at $t = 2500$ ms. Even during the relatively short VBP period,

the effect of doubling the beam divergence is mostly within the uncertainty of the calculation. In consideration of future experiments using VBP and the possibility that time-variable beam divergence will grossly affect power balance calculations, a request for implementing beam divergence as a time variable input has been submitted.[50]
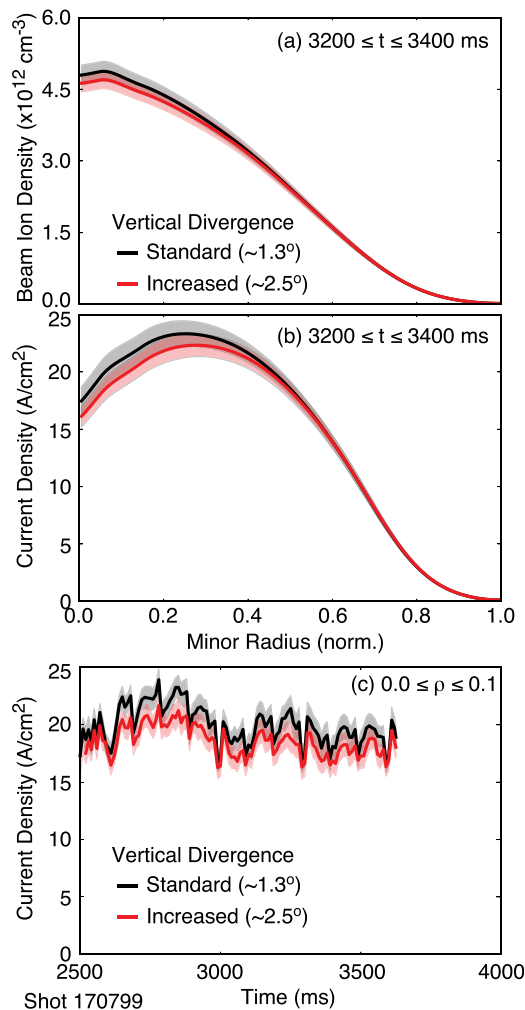

FIG. 15. Beam ion density and beam driven current density for different values of vertical beam divergence. (a) Radial profile of beam ion density for the actual divergence (1.3°, black trace) and an artificially doubled value (2.5°, red trace). (b) Radial profile of current density. (c) Time evolution of the beam driven current density for the two divergence cases.

[1] S. D. Pinches, I. T. Chapman, P. W. Lauber, H. J. C. Oliver, S. E. Sharapov, K. Shinohara, and K. Tani, Phys. Plasmas **22**, 021807 (2015).
[2] W. W. Heidbrink, Phys. Plasmas **15**, 055501 (2008).
[3] W. Heidbrink and G. Sadler, Nucl. Fusion **34**, 535 (1994).
[4] B. N. Breizman and S. E. Sharapov, Plasma Phys. Controlled Fusion **53**, 054001 (2011).
[5] E. D. Fredrickson, M. G. Bell, R. V. Budny, D. S. Darrow, and R. White, Phys. Plasmas **22**, 032501 (2015).
[6] A. Fasoli, D. Testa, T. Panis, A. Klein, J. A. Snipes, J. Sears, M. Gryaznevich, R. Martin, S. D. Pinches, and J.-E. Contributors, Plasma Phys. Controlled Fusion **52**, 075015 (2010).
[7] A. Bortolon, W. W. Heidbrink, G. J. Kramer, J.-K. Park, E. D. Fredrickson, J. D. Lore, and M. Podestà, Phys. Rev. Lett. **110**, 265008 (2013).
[8] K. Nagaoka, T. Ido, E. Ascasíbar, T. Estrada, S. Yamamoto, A. Melnikov, A. Cappa, C. Hidalgo, M. Pedrosa, B. van Milligen, I. Pastor, M. Liniers, M. Ochando, A. Shimizu, L. Eliseev, S. Ohshima, K. Mukai, Y. Takeiri, and the TJ-II Team, Nucl. Fusion **53**, 072004 (2013).
[9] M. V. Zeeland, W. Heidbrink, S. Sharapov, D. Spong, A. Cappa, X. Chen, C. Collins, M. G.-M. noz, N. Gorelenkov, G. Kramer, P. Lauber, Z. Lin, and C. Petty, Nucl. Fusion **56**, 112007 (2016).
[10] S. E. Sharapov, M. Garcia-Munoz, M. A. V. Zeeland, B. Bobkov, I. G. J. Classen, J. Ferreira, A. Figueiredo, M. Fitzgerald, J. Galdon-Quiroga, D. Gallart, B. Geiger, J. Gonzalez-Martin, T. Johnson, P. Lauber, M. Mantsinen, F. Nabais, V. Nikolaeva, M. Rodriguez-Ramos, L. Sanchis-Sanchez, P. A. Schneider, A. Snicker, P. Vallejos, the AUG Team, and the EUROfusion MST1 Team, Plasma Phys. Controlled Fusion **60**, 014026 (2018).
[11] E. D. Fredrickson, E. V. Belova, D. J. Battaglia, R. E. Bell, N. A. Crocker, D. S. Darrow, A. Diallo, S. P. Gerhardt, N. N. Gorelenkov, B. P. LeBlanc, M. Podestà, and N.-U. Team, Phys. Rev. Lett. **118**, 265001 (2017).
[12] D. Gradic, A. Dinklage, R. Brakel, P. McNeely, M. Osakabe, N. Rust, R. Wolf, the W7-X Team, and the LHD Experimental Group, Nucl. Fusion **55**, 033002 (2015).
[13] D. C. Pace, C. Collins, B. Crowley, B. Grierson, W. Heidbrink, C. Pawley, J. Rauch, J. Scoville, M. V. Zeeland, Y. Zhu, and The DIII-D Team, Nucl. Fusion **57**, 014001 (2017).
[14] R. Nazikian, N. N. Gorelenkov, B. Alper, H. L. Berk, D. Borba, R. V. Budny, G. Y. Fu, W. W. Heidbrink, G. J. Kramer, M. A. Makowski, S. D. Pinches, S. E. Sharapov, W. M. Solomon, E. J. Strait, R. B. White, M. A. Van Zeeland, and JET-EFDA Contributors, Phys. Plasmas **15**, 056107 (2008).
[15] C. Murphy, M. Abrahim, P. Anderson, H. Chiu, H. Grunloh, M. Hansink, K. Holtrop, R.-M. Hong, A. Kellman, D. Kellman, P. Mauzey, S. Noraky, C. Pawley, J. Rauch, J. Scoville, M. Van Zeeland, H. Yip, R. Wood, M. Murakami, J. Park, and W. Heidbrink, in *2011 IEEE/NPSS 24th Symposium on Fusion Engineering (SOFE)* (2011), pp. 1–6.
[16] W. Heidbrink, M. V. Zeeland, B. Grierson, C. Muscatello, J. Park, C. Petty, R. Prater, and Y. Zhu, Nucl. Fusion **52**, 094005 (2012).
[17] T. Suzuki, R. Akers, D. Gates, S. Günter, W. Heidbrink, J. Hobirk, T. Luce, M. Murakami, J. Park, M. Turnyanskiy, and the ITPA, "Integrated Operation Scenarios' group members and experts," Nucl. Fusion **51**, 083020 (2011).
[18] J. Scoville, Fusion Sci. Technol. **52**, 398 (2007).
[19] P. Helander, R. J. Akers, and L.-G. Eriksson, Phys. Plasmas **12**, 112503 (2005).
[20] K. H. Burrell, W. P. West, E. J. Doyle, M. E. Austin, T. A. Casper, P. Gohil, C. M. Greenfield, R. J. Groebner, A. W. Hyatt, R. J. Jayakumar, D. H. Kaplan, L. L. Lao, A. W. Leonard, M. A. Makowski, G. R. McKee, T. H. Osborne, P. B. Snyder, W. M. Solomon, D. M. Thomas, T. L. Rhodes, E. J. Strait, M. R. Wade, G. Wang, and L. Zeng, Phys. Plasmas **12**, 056121 (2005).
[21] C. Pawley, B. Crowley, D. Pace, J. Rauch, J. Scoville, D. Kellman, and A. Kellman, Fusion Eng. Des. **123**, 453 (2017).

[22]J. Rauch, D. C. Pace, B. Crowley, R. D. Johnson, D. H. Kellman, C. J. Pawley, and J. T. Scoville, Fusion Sci. Technol. **72**, 500 (2017).

[23]B. G. Penaflor, J. R. Ferron, A. W. Hyatt, M. L. Walker, R. D. Johnson, D. A. Piglowski, E. Kolemen, A. S. Welander, and M. J. Lanctot, in *2013 IEEE 25th Symposium on Fusion Engineering (SOFE)* (2013), pp. 1–4.

[24]B. Crowley, J. Rauch, and J. Scoville, Fusion Eng. Des. **96-97**, 443 (2015), proceedings of the 28th Symposium On Fusion Technology (SOFT-28).

[25]N. H. Brooks, A. Howald, K. Klepper, and P. West, Rev. Sci. Instrum. **63**, 5167 (1992).

[26]D. C. Pace, R. Fisher, M. G. Muñoz, W. Heidbrink, and M. Van Zeeland, Plasma Phys. Controlled Fusion **53**, 062001 (2011).

[27]M. V. Zeeland, N. Gorelenkov, W. Heidbrink, G. Kramer, D. Spong, M. Austin, R. Fisher, M. G.-M. noz, M. Gorelenkova, N. Luhmann, M. Murakami, R. Nazikian, D. Pace, J. Park, B. Tobias, and R. White, Nucl. Fusion **52**, 094023 (2012).

[28]X. Chen, M. E. Austin, R. K. Fisher, W. W. Heidbrink, G. J. Kramer, R. Nazikian, D. C. Pace, C. C. Petty, and M. A. Van Zeeland, Phys. Rev. Lett. **110**, 065004 (2013).

[29]W. W. Heidbrink, E. A. D. Persico, M. E. Austin, X. Chen, D. C. Pace, and M. A. Van Zeeland, Phys. Plasmas **23**, 022503 (2016).

[30]C. S. Collins, W. W. Heidbrink, M. E. Austin, G. J. Kramer, D. C. Pace, C. C. Petty, L. Stagner, M. A. Van Zeeland, R. B. White, Y. B. Zhu, and DIII-D Team, Phys. Rev. Lett. **116**, 095001 (2016).

[31]M. A. Van Zeeland, R. L. Boivin, T. N. Carlstrom, T. Deterly, and D. K. Finkenthal, Rev. Sci. Instrum. **77**, 10F325 (2006).

[32]C. Collins, W. Heidbrink, M. Podestà, R. White, G. Kramer, D. Pace, C. Petty, L. Stagner, M. V. Zeeland, Y. Zhu, and The DIII-D Team, Nucl. Fusion **57**, 086005 (2017).

[33]M. E. Austin and J. Lohr, Rev. Sci. Instrum. **74**, 1457 (2003).

[34]M. García-Muñoz, N. Hicks, R. van Voornveld, I. G. J. Classen, R. Bilato, V. Bobkov, M. Bruedgam, H.-U. Fahrbach, V. Igochine, S. Jaemsae, M. Maraschek, K. Sassenberg, and ASDEX Upgrade Team, Phys. Rev. Lett. **104**, 185002 (2010).

[35]Y. Todo, M. V. Zeeland, A. Bierwage, and W. Heidbrink, Nucl. Fusion **54**, 104012 (2014).

[36]J. Varela, D. Spong, and L. Garcia, Nucl. Fusion **57**, 046018 (2017).

[37]C. T. Holcomb, W. W. Heidbrink, J. R. Ferron, M. A. Van Zeeland, A. M. Garofalo, W. M. Solomon, X. Gong, D. Mueller, B. Grierson, E. M. Bass, C. Collins, J. M. Park, K. Kim, T. C. Luce, F. Turco, D. C. Pace, Q. Ren, and M. Podesta, Phys. Plasmas **22**, 055904 (2015).

[38]B. Wan, J. Li, H. Guo, Y. Liang, G. Xu, and X. G, for the EAST Team, and I. Collaborators, Nucl. Fusion **53**, 104006 (2013).

[39]W. Heidbrink, M. V. Zeeland, M. Austin, E. Bass, K. Ghantous, N. Gorelenkov, B. Grierson, D. Spong, and B. Tobias, Nucl. Fusion **53**, 093006 (2013).

[40]see http://transpweb.pppl.gov/development-1 for A collection of documents detailing TRANSP calculations and abilities, 2017.

[41]I. Klimek, M. Cecconello, M. Gorelenkova, D. Keeling, A. Meakins, O. Jones, R. Akers, I. Lupelli, M. Turnyanskiy, G. Ericsson, and the MAST Team, Nucl. Fusion **55**, 023003 (2015).

[42]O. Meneghini, S. Smith, L. Lao, O. Izacard, Q. Ren, J. Park, J. Candy, Z. Wang, C. Luna, V. Izzo, B. Grierson, P. Snyder, C. Holland, J. Penna, G. Lu, P. Raum, A. McCubbin, D. Orlov, E. Belli, N. Ferraro, R. Prater, T. Osborne, A. Turnbull, and G. Staebler, Nucl. Fusion **55**, 083008 (2015).

[43]G. McKee, R. Ashley, R. Durst, R. Fonck, M. Jakubowski, K. Tritz, K. Burrell, C. Greenfield, and J. Robinson, Rev. Sci. Instrum. **70**, 913 (1999).

[44]M. Podestà, M. Gorelenkova, D. Darrow, E. Fredrickson, S. Gerhardt, and R. White, Nucl. Fusion **55**, 053018 (2015).

[45]M. Podestà, M. Gorelenkova, N. N. Gorelenkov, and R. B. White, Plasma Phys. Controlled Fusion **59**, 095008 (2017).

[46]B. Geiger, M. Weiland, A. Mlynek, M. Reich, A. Bock, M. Dunne, R. Dux, E. Fable, R. Fischer, M. Garcia-Munoz, J. Hobirk, C. Hopf, S. Nielsen, T. Odstrcil, C. Rapson, D. Rittich, F. Ryter, M. Salewski, P. A. Schneider, G. Tardini, and M. Willensdorfer, Plasma Phys. Controlled Fusion **57**, 014018 (2015).

[47]D. C. Pace, M. E. Austin, E. M. Bass, R. V. Budny, W. W. Heidbrink, J. C. Hillesheim, C. T. Holcomb, M. Gorelenkova, B. A. Grierson, D. C. McCune, G. R. McKee, C. M. Muscatello, J. M. Park, C. C. Petty, T. L. Rhodes, G. M. Staebler, T. Suzuki, M. A. Van Zeeland, R. E. Waltz, G. Wang, A. E. White, Z. Yan, X. Yuan, and Y. B. Zhu, Phys. Plasmas **20**, 056108 (2013).

[48]S. Zhou, W. W. Heidbrink, H. Boehmer, R. McWilliams, T. Carter, S. Vincena, S. K. P. Tripathi, P. Popovich, B. Friedman, and F. Jenko, Phys. Plasmas **17**, 092103 (2010).

[49]K. Gustafson, P. Ricci, A. Bovet, I. Furno, and A. Fasoli, Phys. Plasmas **19**, 062306 (2012).

[50]TRANSP User Group, Meeting held at the American Physical Society - Division of Plasma Physics Conference, Milwaukee, WI, 23-27 October 2017.